Egyptian Journal of Chemistry
http://ejchem.journals.ekb.eg/

Scale-up and Practical Application of Waste Biomass for water Treatment

Sahar Shaarawy [a*], Emad K. Radwan [b], Amira El-Shafei [a*]
[a] Pre-Treatment and Finishing of Cellulosic Fabric Department, Textile Research Division, National Research Center, 33 El-Buhoth St, Dokki, Cairo 12311, Egypt
[b] Department of Water Pollution Research, National Research Centre, 33 El Bohouth St, Dokki, Giza 12622, Egypt

In Loving Memory of Late Professor Doctor ""Mohamed Refaat Hussein Mahran""

Abstract
In this study comparison for wastewater treatment takes place between corn straw (CS) waste and microcrystalline cellulose (MCC) as two different reasonably priced biomass subjected to graft via acrylic acid. The grafting polymerization for two biomass individually and Acrylic Acid (AA) was done via ammonium persulfate as initiator and N,N-methylenebisacrylamide as a crosslinking agent, to concoct CS-g-AA&MCC-g-AA. The structure and properties of the resulting product were characterized by add-on percent, FTIR, X-ray diffraction, and SEM. The grafting conditions were studied and the final product was subjected to an adsorption study. The results of the adsorption study revealed that grafting PAA onto MCC even at the lowest concentration improved the adsorption efficacy significantly. The optimum conditions for the removal of RhB are pH 6, and 1.0 g/L where 93% was removed in 90 min using MCC-g-PAA0.5 and 90% was removed in 90 min using CS-g-AA4. The adsorption kinetics and isotherm studies illustrated that the adsorption process wasn't simple. Comparing the Langmuir theoretical monolayer saturation capacity of CS-g-AA4 (233 mg/g) showed its high potential as an adsorbent for the treatment of dye-contaminated wastewater.
Keywords. Corn Waste; Microcrystalline cellulose; biomass; grafting polymerization; Wastewater treatment; adsorption; kinetic and isotherm models.

1. Introduction

Following the immense environmental damage caused by the manufacturing techniques utilized in current systems, which result in accumulating carbon emissions, global warming, and the creation of new non-degradable components. Scientists have taken action to lessen environmental contamination as a result of these worries, which impede the life cycle of many species on Earth. To get over these obstacles, scientists have created green-designed materials, which offer several benefits like being biodegradable, inexpensive, lightweight, renewable, chemically inert, and compatible with the majority of synthetic plastic materials. [1-4]. The effort to improve the characteristics of biocomposite materials is still ongoing. Biocomposite materials can be readily derived from a variety of agricultural lagging materials, including kenaf, hemp, cassava, wheat, jute, and corn. [5].

Agricultural wastes are more valuable than materials from other sources because of their characteristics—chemical, physical, and quantity—and quality. They have varied degrees of polymerization and a high cellulose content in their fibers [6]. Moreover, the degree of crystallinity, density, and porosity all affect how the manufacturing process is varied. Corn is one of the most important lignocellulosic crops cultivated. after rice and wheat which are rich in starch. Corn is regarded as a high-fiber and high-starch food. The wet milling technique separates the maize husk fiber, cellulose, hemicellulose, and gluten from the granules. By drying, crushing, and sieving the stems and leaves, corn stalk (CS) and husk can be extracted [7]. Depending on the characteristics of the material used as the matrix and the chemical interaction formed between the filler and the matrix, the percentage of corn in the biocomposite varies dramatically for each composition. To attain ideal mechanical, thermal, and chemical characteristics, an experimental determination of the appropriate composition is required. The characteristics often start to decline beyond a certain point or percentage of corn load, and adding more materials or undergoing chemical or thermal treatment is necessary to reverse the decline. Additionally, corn is combined with other materials to improve their qualities.

*Corresponding author e-mail: sahar.shaarawy@yahoo.com; (Sahar Shaarawy
Receive Date: 26 December 2023, Revise Date: 31 January 2024, Accept Date: 18 February 2024
DOI: 10.21608/ejchem.2024.258353.9085

Acrylic acid grafting onto corn waste can be a promising approach for water treatment. Corn waste, such as corn stalks, husks, or cobs, is a renewable and abundant agricultural residue that can be utilized as a low-cost and sustainable adsorbent material. Grafting acrylic acid onto corn waste involves modifying the surface of the waste material by attaching acrylic acid molecules to it. This modification enhances the adsorption capabilities of the corn waste, allowing it to effectively remove noxious waste from water.

Here are some key benefits and considerations for using acrylic acid graft corn waste for water cure:

1- Adsorption Capacity: Acrylic acid grafting can increase the surface area and introduce functional groups on the corn waste, which can enhance its adsorption capacity. The grafted material can effectively adsorb various pollutants, including organic compounds, heavy metals, and dyes, from water.
2- Renewable and Low-Cost Material: Corn waste is readily available as an agricultural byproduct, making it an attractive choice for water treatment applications. It offers a sustainable alternative to synthetic adsorbents and can be obtained at a relatively low cost, reducing overall treatment expenses.
3- Eco-Friendly Approach: Utilizing corn waste as an adsorbent promotes the utilization of agricultural residues and reduces waste generation. This approach aligns with the principles of sustainability and environmental conservation.
4- Regeneration and Reusability: Depending on the specific grafting method and adsorbent characteristics, acrylic acid graft corn waste can often be regenerated and reused. This can be beneficial for long-term applications and cost-effectiveness.
5- Optimization and Performance: The efficiency of acrylic acid graft corn waste as a water treatment material depends on several factors, including the grafting process parameters, the concentration and nature of pollutants, and the operating conditions. Optimization studies are necessary to determine the optimal grafting conditions and maximize the adsorption performance.
6- Compatibility and Application: Acrylic acid graft corn waste can be used in various water treatment applications, such as the removal of organic pollutants from industrial wastewater or the treatment of contaminated groundwater. Compatibility with different water matrices and pollutants needs to be evaluated to ensure effective performance.

There are four primary categories of biomass: wood, forestry residue, industrial waste, municipal trash, and agricultural waste. Biomass has long been investigated as an adsorbent in wastewater treatment due to its abundance, low cost, and several functional groups. Because of their short regeneration cycle, effectiveness, availability, chemical stability, environmental friendliness, and affordability, agricultural waste in particular can be employed as adsorbents for water remediation [8]. They easily absorb dye and heavy metal ions due to their porous structure, large specific surface area, and variety of functional groups [9]. Adsorbents such as sawdust [10], sugarcane bagasse [11], rice husk [12], rice straw [13], maize straw, wheat straw [14], and wood shavings [15] have been utilized in place of raw agricultural solid wastes and waste products from the forest industry. Because of their low cost and physicochemical properties, these materials are readily available in large quantities and may have promise as sorbents [16].

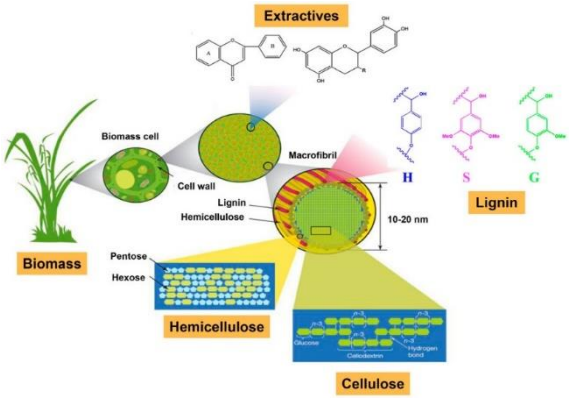

Scheme 1. Flow diagrams of corn waste content and extraction methods

Corn waste and its derivatives are an inexpensive and safe source of raw materials for the production of inexpensive adsorbents that could be effective in removing contaminants from wastewater. This biopolymer presents an intriguing alternative as an adsorbent due to its unique qualities (renewable, abundant, and biodegradable raw resource) and qualities like high reactivity and chemical stability, resulting from the presence of chemically reactive hydroxyl groups in polymer chains [17]. These properties enable the chemical modification of corn waste to meet various requirements. Following alteration, starches exhibit large pore volume, high specific area, and appropriate expansion, all of which can improve their adsorption capacity. This indicates that modified corn wastes are better suited to use as catalytic carrier materials or as an adsorbent for dyes and heavy metals [18].

Furthermore, dyes and heavy metals can be successfully removed from synthetic wastewater by using MCC-based materials, which are a common carbohydrate polymer derived from lignocellulosic biomass, as efficient adsorbents. With the Langmuir

isotherm and pseudo-second-order primarily reported as the best-fit models for the generated equilibrium and kinetic data, respectively, MCC-based materials performed exceptionally well in the adsorption of dyes and heavy metals, pointing to the homogeneous distribution of adsorption sites as well as the formation of monolayer adsorbate on their surfaces [19].

Water pollution has gained increasing attention in recent years. It is now admitted that untreated and/or improperly treated industrial wastewater discharges are the main source of contamination of water bodies [20-21]. The wastewater of dye-consuming industries raises major environmental concerns owing to its large amount, widespread, complexity, and inclusion of several bio-recalcitrant dyes [22,20]. The contamination of water sources by synthetic organic dyes is visually unappealing, hinders sunlight from penetrating the water leads to serious damage to aquatic life, harms living organisms, and can result in mutations, cancer, allergic dermatitis, skin irritation, and nervous system damage [22,23,20]. Therefore, the treatment of dye-contaminated wastewater is a topic that poses a true challenge and researchers are constantly interested in it.

Various treatment techniques including chemical, physical, and biological methods have been investigated to treat dye-contaminated [20-22,24]. However, adsorption is widely used among other treatment techniques as a result of its cost-effectiveness, technical feasibility, simplicity, and high efficiency [20,22].

The present work is undertaken to synthesize innovative biomass polymeric products and to characterize them as a prerequisite for their utilization in the area of water treatment. In this research, the combination of [AA] acrylic acid, methylene bisacrylamide, and [CS] corn waste and [MCC] in crosslinked-based adsorbents offers a versatile and sustainable approach for water treatment. It capitalizes on the adsorption properties of acrylic acid, the cross-linking capabilities of methylene bisacrylamide, and the natural filler attributes of corn waste. We also used MCC Grafted with acrylic acid and the presence of, methylene bisacrylamide as a comparison for water treatment application. The adsorption efficacy of the prepared materials was assessed and compared using Rhodamine B (RhB) as a model for dyes. RhB is a highly water-soluble basic cationic dye belonging to the xanthene group of dyes. RhB was selected as a model in this study because of its extensive use in leather, paper, printing, paint, and textile industries in addition to its usage as a biomarker and tracer [20,22,25]. RhB resists photolysis, thermolysis, and biodegradation [22] and is toxic to many organisms, and potential mutagen and carcinogen [20,25]. Therefore, the removal of RhB from the aqueous solution is urgently required. The adsorption assay included evaluating the effect of experimental conditions such as the initial pH of the solution, amount of used material, and contact time. Furthermore, the adsorption kinetics and isotherms were investigated and analyzed using the common models.

Further research and development in this area can contribute to the advancement of effective and environmentally friendly water treatment solutions. the aforementioned polymeric products were characterized by Fourier transform infrared (FTIR) spectroscopy and scanning electron microscopy (SEM), X-ray diffraction.

2. Materials and methods

2.1. Materials

MCC was purchased from Chemicals LTD. Co. (Korea). Acrylic acid was supplied from Fluka Co. (Switzerland). MBA, NaOH, sodium carbonate, and HCl were purchased from Sigma-Aldrich Co. (Germany). Ammonium persulphate was purchased from AlPHA CHEMICAL Co. (India). Corn waste was collected from the residue of agricultural waste. Other chemicals used in this study were of analytical reagent grade and used without further purification.

2.1.1 Preparation of CS-g-AA and MCC-g-AA

Dry corn stalks [CS] were ground and sieved using a 40-mesh sieve. Then, the resulting [CS] crash-washed via alkaline media with 15% NaOH solution at 55 ^{0}C in a water bath for 0.5 h. The resulting alkaline corn waste was washed with distilled water, and dried.

The graft polymerization reaction of CS and MCC chain with vinyl monomer (AA) in the presence of Am PS as an initiator and MBA as a crosslinking agent was used to prepare the CS-g-AA and MCC-g-AA. The synthesis process for MCC-g-AA and CS-g-AA is shown in Scheme 1. A mechanical stirrer was used to continuously stir a solution containing varying concentrations of acrylic acid in 30 milliliters of deionized water (DI). An electrical bath was used to maintain a constant reaction temperature. Using 0.01 M NaOH, the pH of the reaction medium was brought to 4, and then various concentrations of AA were added to the CS or MCC solution. The CS/MCC/AAm suspension was then mixed with a constant concentration of MBA (0.15 g/10 mL DI) and kept at 78°C for 4 hours while being stirred and heated. The resulting composite grafted materials were filtered out after being cleaned off with a 20/80 ethanol/water mixture. Ultimately, the resulting grafted products were collected, dried at 90 °C, and stored for additional research. The add-on % of the grafted product is displayed in Figure 4.

2. 2. Characterization

2.2.1. FTIR spectroscopy analysis

JASCO FT-IR 6100 spectrometer (Tokyo, Japan) was used to record the FTIR spectra of the differently prepared samples. The measurements were carried out within the range of 4000–400 cm^{-1}, with 60 scans and a resolution of 4 cm^{-1}.

2.2.2. X-ray diffraction (XRD) analysis

Panalytical Empyrean X-ray diffractometer (PANalytical, Netherlands), with an angle of incident monochromatic X-ray in the range of 2θ=5–80°, was used to analyse the lyophilized NCs and NC-Ag bio- nanocomposites samples and dry films of chitosan bio-nanocomposite under investigation.

2.2.3. Morphological analysis Quanta FEG-250 (Waltham, MA, USA)

scanning electron microscope, at a voltage of 20 kV, was used for imaging and elemental analysis, by energy-dispersive X-ray spectroscopy, of the films. The transmission electron micrographs of NCs and NC-Ag bio-nanocomposites were captured with high-resolution JEOL JEM-2100 (Japan). The ONC, SNC, and PNC suspensions were dried on a microgrid covered with a thin carbon film (≈200 nm). To enhance the microscopic resolution, the precipitated ONC, SNC, and PNC were dyed with a 2% uranyl acetate solution. On the other hand, the precipitated ONC-Ag, SNC-Ag, and PNC-Ag bio-nanocomposites were left without dyeing.

2.2.4. Instruments

The batch adsorption studies were performed using an orbital shaking incubator (DAIHAN Thermo Stable™ IS-30, Korea) and the concentration of RhB was measured using a double-beam UV-visible spectrophotometer (JASCO V730, Japan).

2.2.4.1 Adsorption study

The adsorption efficacy of the prepared materials was assessed using RhB as the model substrate. Before the experiments, RhB solutions with different concentrations were prepared and their visible spectrum was recorded. Figure 1 shows the obtained spectrum of 10 mg/L RhB solution, as an example, and the calibration curve. The maximum absorption wavelength (λ_{max}) was observed at 553 nm and the calibration curve exhibited excellent linearity (R^2 = 0.9995) up to 100 mg/L. In the adsorption experiment, the weight of the material was agitated with RhB solution at 200 rpm and room temperature. After certain contact times, samples were withdrawn and the concentration of RhB was measured. The percentage of RhB removed (R%) was calculated by Equation 1.

$$R\ (\%) = \left(1 - \frac{C_t}{C_i}\right) \times 100 \qquad (1)$$

where C_t is the concentration in mg/L of RhB at contact time t, and C_i is the initial concentration in mg/L of RhB.

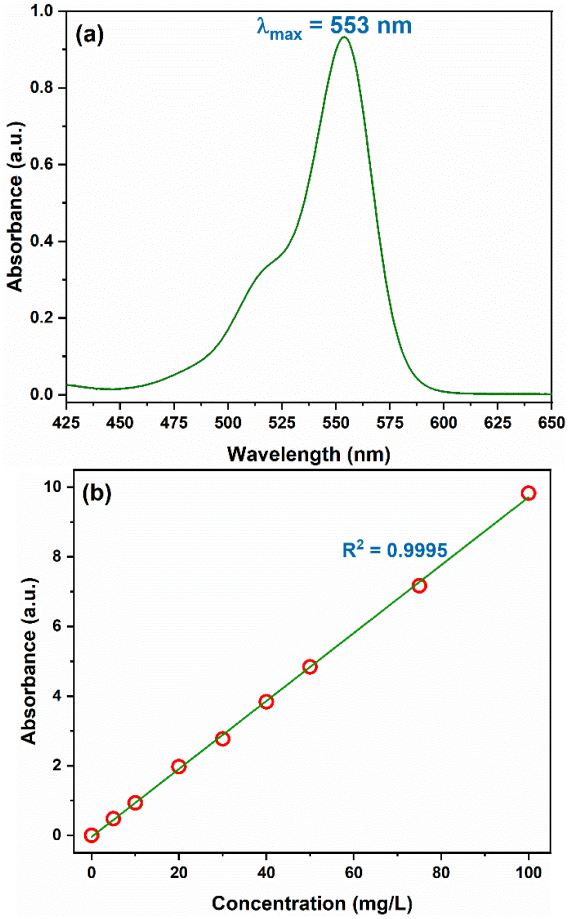

Figure 1. (a) Visible spectrum of 10 mg/L RhB solution and (b) calibration curve.

The adsorption study included assessing and comparing the efficacy of the different prepared materials, assessing the changes of R% with changing the initial pH of RhB solution and the amount of the material, adsorption kinetics, and adsorption isotherm. The effect of the initial pH (pHi) of the RhB solution was studied by adjusting the pH to 2.0, 4.0, 6.0, 8.0, or 10.0 using 0.1 M NaOH or 0.1 M HCl and performing the adsorption experiments. After identifying the optimum pHi, different amounts (0.50-1.00 g/L) of the best-performing material were agitated with RhB solution pre-adjusted to the optimum pHi to explore the effect of the amount of material. The kinetics of adsorption were analyzed using the non-linear forms of the widely applied pseudo-first-order (PFO) [26] and pseudo-second-order (PSO) [27] equations. At first, the amount of RhB adsorbed onto a gram of the material (q_t, mg/g) at contact time t (min.) was calculated by equation 2 and then applied in the PFO and PSO equations, equations 3 and 4 respectively.

$$q_t = (C_i - C_t)\frac{V}{m} \quad (2)$$

$$q_t = q_e\,(1 - e^{-k_1 t}) \quad (3)$$

$$q_t = \frac{k_2 q_e^2 t}{1 + k_2 q_e t} \quad (4)$$

where qe is the amount of RhB adsorbed onto a gram of the material at equilibrium (qe, mg/g), k_1 (1/min) and k_2 (g/mg.min) are the rate constants of the PFO and PSO reactions, respectively.

In the isotherm study, the initial concentration of RhB was changed over the range of 5-100 mg/L, and the obtained data was analyzed by the non-linear forms of Freundlich [28] and (Langmuir 1918)[29] models (equations 5 and 6, respectively).

$$q_e = K_F\, C_e^{1/n} \quad (5)$$

$$q_e = \frac{q_L K_L C_e}{1 + K_L C_e} \quad (6)$$

where K_F (mmol(1-1/n)L(1/n)/mol) and n (–) are Freundlich constants, q_L (mmol/g) is the Langmuir theoretical monolayer saturation capacity, and K_L (L/mmol) is Langmuir constant.

The experimental data were fitted to the kinetics and isotherm models using OriginPro 2021 software. The accuracy of the data predicted by the model was judged based on the value of both the determination coefficient (R^2, equation 7), and chi-square (χ^2, equation 8). The higher value of R^2 and lower value of χ^2 indicate excellent matching between the practical and model-predicted data.

$$R^2 = \frac{\sum \left(q_{e,cal} - \bar{q}_{e,exp}\right)^2}{\sum \left(q_{e,cal} - \bar{q}_{e,exp}\right)^2 - \sum (q_{e,cal} - q_{e,} \quad (7)$$

$$\chi^2 = \sum_{i=1}^{N} \left[\frac{\left(q_{e,exp} - q_{e,cal}\right)^2}{q_{e,cal}}\right] \quad (8)$$

where $q_{e,cal}$ and $q_{e,exp}$ are the model predicted and experimental equilibrium adsorption capacity, respectively, $\bar{q}_{e,exp}$ is the average of $q_{e,exp}$, and N is the number of experimental points.

3. Results and discussion

While research studies have demonstrated the potential of acrylic acid graft corn waste and MCC for water treatment, scaling up the production and application of this material requires further development and optimization. Considerations such as cost-effectiveness, large-scale grafting methods, and practical implementation need to be addressed for real-world applications. It's important to note that the effectiveness of acrylic acid graft corn waste for water treatment can vary depending on the specific pollutants, concentration levels, and water quality parameters discussed below. Therefore, thorough testing and evaluation should be conducted to assess the performance of the material under the intended water treatment conditions.

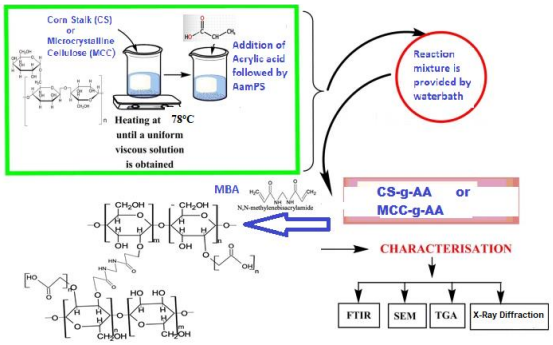

Scheme 1. Flow diagrams of synthesis methods mechanism of preparation CS-g-AA and MCC-g-AA.

Evidence of Graft Polymerization Characterization of the Functional Group of the Copolymers by FTIR Spectroscopy

In addition to the ingredients utilized in grafting, such as AA and MBA, Figure 2 displays the FTIR spectra of the CS before and after the grafting. Figure 3 displays the grafted and native MCC. There is a larger peak at 3400 cm-1 that originates from O–H valence vibrations and a smaller peak at 2925 cm-1 that originates from C–H valence vibrations. C-O-C stretching is described by wave numbers at approximately 1153, 1078, and 1023 cm-1 [30]. The OH valence band of the CS group and the NH valence band of the MBA overlap in the CS-g-AA example, resulting in a peak at 3730 cm-1 that rests atop a peak that occurs at roughly 3670 cm-1. about at 570, 764, 860, The strength and shape of the grafted CS group's vibrations alter, suggesting that the OH of the CS groups underwent changes during the reaction.

Therefore, the existence of these extra peaks in the grafted cellulose instance relative to CS indicates that the grafting of poly (acrylic acid) chains onto CS was successful. The FTIR spectrum of CS-g-AA displays the following bands corresponding to the monomer: C-O valence vibrations at 1295 and 1170 cm-1, C=C double bond valence vibrations at 1650 cm-1, C-H bond valence vibrations (CH_3) at 2928 cm-1, and OH group valence vibrations at roughly 3420 cm-1. The effective grafting of AA onto the treated CS was verified by the FTIR analysis.

Figure 3. MCC shows the O–H stretching absorption in the range of 3650–3000 cm-1 (wide, s), the C–H stretching at 2900 cm-1, and the wave number of 1025 for the C–O stretching in addition to the previously shown figures of the AA and MBA peaks. All of the distinctive absorption peaks associated with MCC were visible in the FTIR spectra of MCC-g-AA. Furthermore, the C=O stretching, which is a feature of the -COO group found in AA, is indicated by the peak at 1728 cm-1. The evidence supporting the grafting of acrylic acid onto the MCC backbone was the new absorption

band detected at 1728 cm-1. Additionally, as the amount of graft grew, so did the peak intensities of C-H stretching at 2900 cm-1, C=O stretching at 1728 cm-1, and C=O stretching at 1025 and 1165 cm-1.

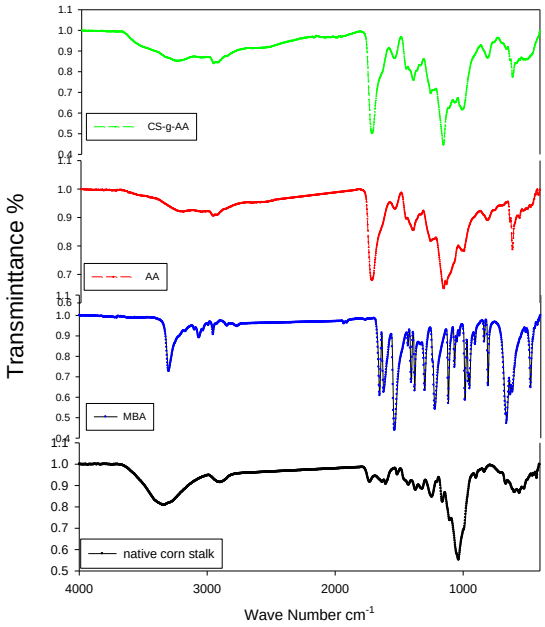

Figure 2. FTIR of CS, AA, MBA, CS-g-AA.

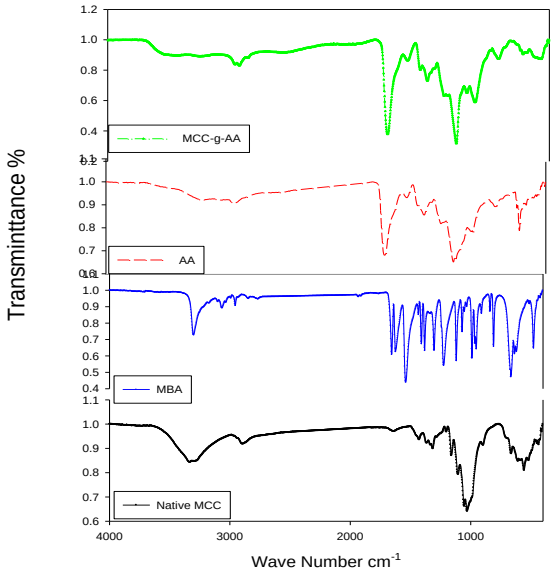

Figure 3. MCC, AA, MBA, MCC-g-AA.

Effect of Acrylic Acid Concentration on % add-on

Figure 4 shows the Effect of acrylic acid concentration on the % add-on of the grafted product either CS-g-AA or MCC-g-AA. The figure shows at low levels of monomer dosage there are slight increase in the add-on level. By increasing monomer concentration and ammonium persulfate initiator are too many radicals that cause premature terminations as well as increased homopolymer formation. The reason for the latter is not fully clear but it is speculated that in a further stage of the reaction, there may be a limited number of grafting sites available from the backbone carbohydrate, perhaps due to steric hindrance. The optimum value is different for each specific grafting system so it can only be determined by experiments. We increase the AA concentration until reaches a suitable concentration for dye adsorption.

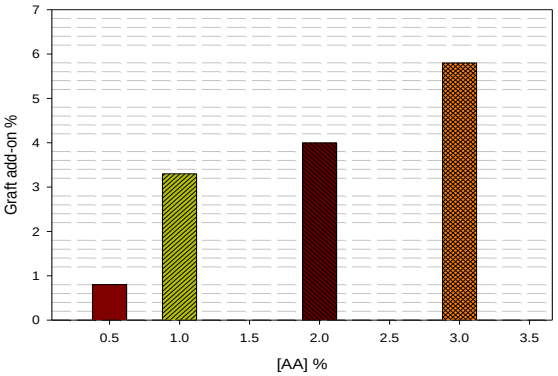

Figure 4. Effect of Acrylic Acid Concentration on % add-on

Scanning Electron Microscope (SEM)

SEM was used to examine the morphological characteristics of the CS, grafted CS-g-AA, and MCC, as well as the grafted MCC-g-AA. A typical surface morphology for both CS and CS-g-AA is shown in Figs. [5 a,b], [6 a,b]. The surface of CS is more asymmetrical, rugged, and porous. Grafted corn waste has pores, which raises the likelihood that metal ions may get trapped and adsorbed onto the surface. The surface roughness of the modified cellulose increased, as seen by the SEM images of the adsorbent (Fig. 6a.b). The SEM pictures (Fig. 6a.b) demonstrate how entirely the AA layers cover the cellulose's surface. This shows that the synthesis was successful and that the AA treatment increased the surface area.

Scanning electron microscopy was used to study the surface appearances of MCC and MCC-g-AA, as illustrated in Figure [6 a,b]. MCC had a flat surface, as Figure 6(b) illustrates. Nevertheless, as Figure 6(b) illustrates, there were numerous aggregations of modified cellulose following polymerization. Additionally, as a result of microphase separation, the surfaces of MCC-g-AA resembled the fish scales depicted in Figure 6(b). Figure 6(b) depicted the pore structure of MCC. The pores' diameter ranged from few nanometers to dozens of nanometers, and their surface was covered with a large number of irregular pores. But upon copolymerization, the holes vanished and were replaced by an uneven stripe, as seen in Figure 6(b). There is a crosslinking structure in the modified MCC.

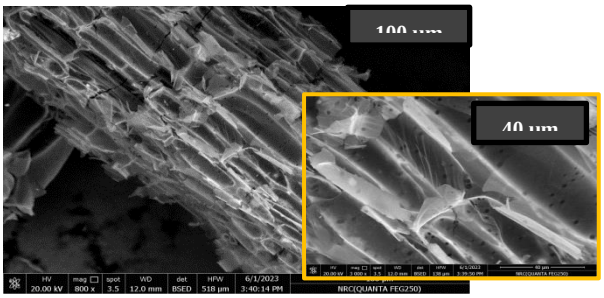

Fig 5 a Raw Corn Stake

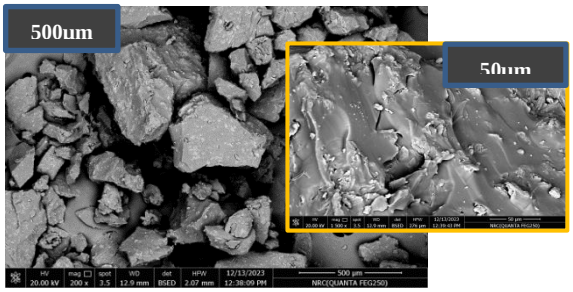

Fig 5b CS-g-AA

Figure 5 (a,b) SEM micrographs of the prepared, s-g-AA before (a) and after grafting (b).

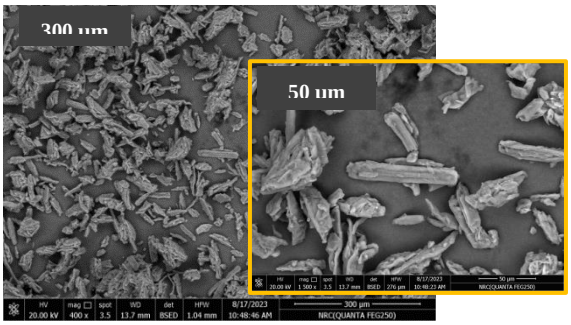

Fig 6a MCC Raw

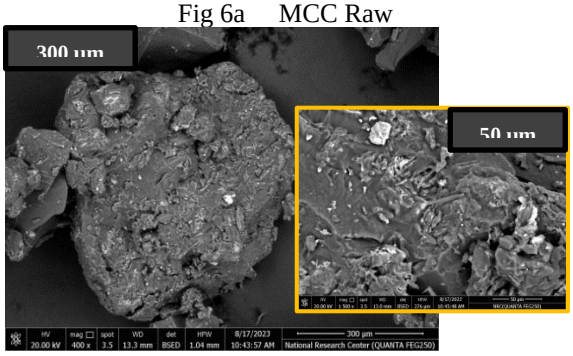

Fig 6 b MCC-g-AA

Figure 6 a,b SEM micrographs of the prepared, MCC-g-AA before (a) and after grafting (b).

X-ay Diffraction

MCC –g-AA prepared using low feed concentration (0.5% sample) was selected for further characterization using XRD analyses. The crystal structures of Raw MCC and MCC –g-AA are shown in Fig. (7a,b,c). The XRD patterns (Fig. 7a,b) of both samples exhibit peaks at 2θ=16°, 22° and 35°. These peaks are consistent with the position of diffraction peaks of the reference cotton cellulose/polymorph structure Although there is not much difference in peak positions of the two samples, the diffraction peaks of the Raw MCC are less intense than the grafted MCC. This phenomenon is probably due to the introduction of vinyl groups onto the backbone.

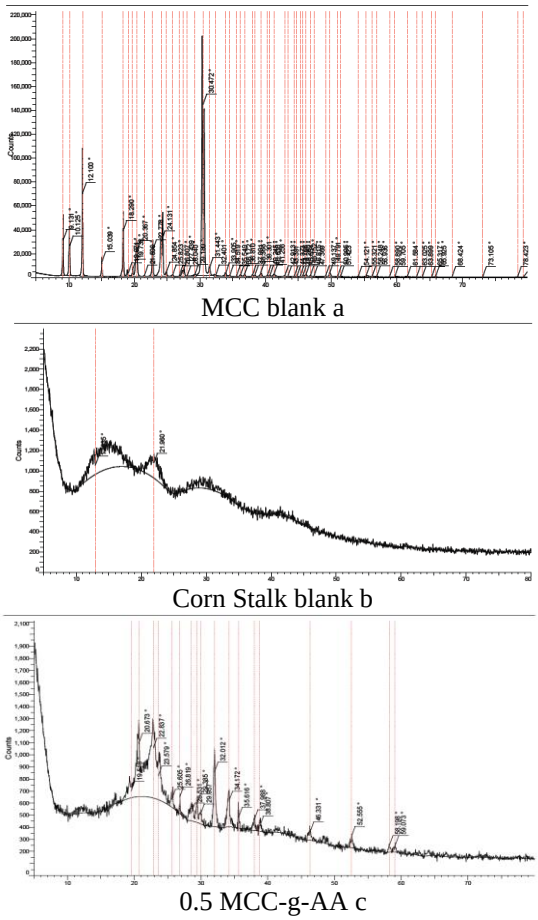

MCC blank a

Corn Stalk blank b

0.5 MCC-g-AA c

Fig. 7. (a,b,c) XRD patterns of MCC blank,CS Raw,).5MCC-gAA

Adsorption study

The adsorption efficacy of the different prepared materials toward RhB was assessed and compared. Figure 8 displays the obtained results.

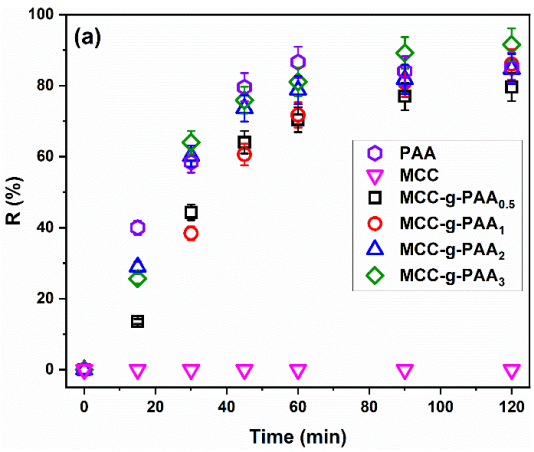

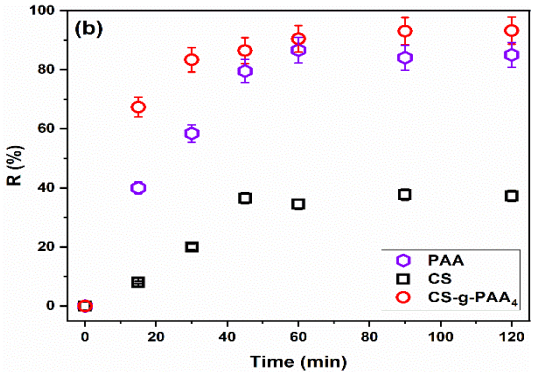

Figure 8. Comparing the adsorption efficacy of the different prepared materials toward (a) MCC-g-PAA (C_i 10 mg/L, dosage 1.0 g/L, pH_i 6) and (b) CS-g-PAA (C_i 10 mg/L, dosage 1.0 g/L, pH_i 6).

Figure [8 a & b] shows that pure MCC cannot adsorb RhB. On the contrary, pure PAA can effectively remove RhB where 85% was removed using 1 g/L after 2 hr. Figure [8 a] illustrates that grafting AA onto MCC even with the lowest concentration (sample MCC-g-$PAA_{0.5}$) has a tremendous improving effect on the adsorption efficacy of MCC. The removal of RhB using 1 g/L of MCC-g-$AA_{0.5}$ reached 77% after 90 min and increased to 80% after 120 min. Increasing the concentration of grafted AA brought about a slight increase in the R%. The R% was 86%, 84%, and 91% for MCC-g-AA_1, MCC-g-AA_2 and MCC-g-AA_3, respectively. The enhancement in R% associated with increasing the AA concentration is insignificant, therefore, the sample MCC-g-$AA_{0.5}$ was selected for further study. On the other side, Figure [8 b] shows that grafting AA onto CS improved the adsorption efficacy of CS toward RhB, the R% using 1 g/L increased from 38% for the pure CS to 93% for CS-g-AA_4 in 2 hr. Consequently, the sample CS-g-AA_4 was used to evaluate its adsorption efficacy under different conditions.

Generally, the surface charge of the adsorbent and the ionic form of the adsorptive depend on the pH_i of the solution [21]. RhB has a pK_a of 3.7, thus at pH < 3.7 it exists mainly as a cationic molecule (RhB^+) whereas at pH > 3.7 the carboxylic group deprotonates forming the zwitterionic molecule (RhB±).[31] Figure 9 represents these two forms of RhB.

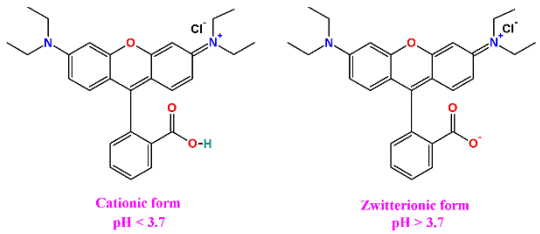

Figure 9. Molecular structures of RhB at different pHs.

As illustrated in [Figure 10a], the removal of RhB by MCC-g-$AA_{0.5}$ was 80% at pH_i 2 and increased to 96% at pH_i 4. An additional increase in the RhB solution pH_i to 6 and 8 has a slight effect on R% where it insignificantly dropped to 88% and 89%, respectively, but at pH_i 10 the R% significantly drops to 65%. These results can be explained in terms of electrostatic interactions. At highly acidic or alkaline pHs, repulsion forces rules leading to low R% while at pH 4-8 attraction forces rules leading to higher R%. In more detail, at pH_i 2 the oxygen-containing functional groups of MCC-g-$AA_{0.5}$ become protonated and repulse the cationic RhB whereas at pH_i 10 these functional groups become negatively charged and repulse the carboxylate group of RhB. In addition, at pH_i 10 the zwitterionic form of RhB aggregates producing a macromolecule that is hard to adsorbed [32,33]. At pH_i 4, the protonated oxygen-containing functional groups of MCC-g-$AA_{0.5}$ attract the carboxylate group of RhB resulting in the highest observed R%. While at pH_i 6 and 8 the magnitude of protonation of these groups slightly decreased, consequently the attraction forces are weakened resulting in the observed insignificant drop in R%. For CS-g-AA_4 (Figure 10 b), the R% of RhB is not significantly affected by the pH_i. This observation suggests that mechanisms other than electrostatic interactions are probably included in the adsorption of RhB onto CS-g-PAA_4. Based on the results of the pH_i effect it can be concluded that the optimum pH_i is the natural pH of the RhB solution (pH 6).

[Figure 10 c & d] discloses that the amount of both MCC-g-$AA_{0.5}$ and CS-g-AA_4 affects the removal of RhB in a similar and traditional way. The R% increases as the dosage of either MCC-g-$AA_{0.5}$ or CS-g-AA_4 increases. The R% was 75%, 86% and 96% using 0.50 g/L, 0.75 g/L, and 1.00 g/L of MCC-g-$AA_{0.5}$. Likewise, the R% was 82%, 90% and 93% using 0.50 g/L, 0.75 g/L, and 1.00 g/L of CS-g-AA_4. This outcome makes sense as adding more material increases both the accessible surface area and the number of adsorption sites.[34] Another note from [Figure 10 c & d] is that the increase of R% with dosage was more significant for MCC-g-$AA_{0.5}$ relative to CS-g-AA_4.

Contact time is a key parameter in evaluating an adsorbent's efficiency. Analyzing the effect of contact time on RhB R% [Figure 10 c & d] reveals that the R% increases stepwisely with contact time for both MCC-g-$AA_{0.5}$ and CS-g-AA_4. Moreover, the adsorption of RhB by CS-g-AA_4 was faster than MCC-g-$AA_{0.5}$, and the R% at the beginning of contact time was considerably higher. These observations infer that compared to MCC-g-$AA_{0.5}$, CS-g-AA_4 contains more adsorption sites, and/or RhB accession to adsorption sites of CS-g-AA_4 is easier.

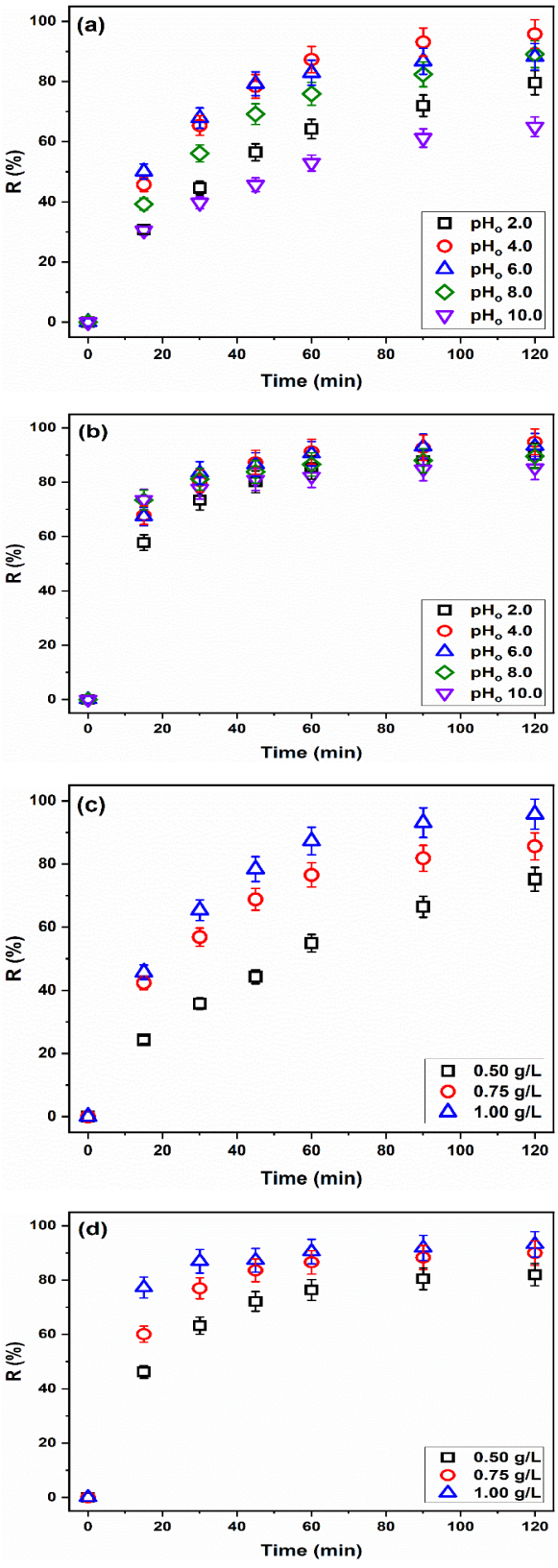

Figure 10. Changes of R% with solution pH$_o$ (a) MCC-g-AA$_{0.5}$ (C$_i$ 10 mg/L, dosage 1.0 g/L) & (b) CS-g-AA$_4$ (C$_i$ 10 mg/L, dosage 1.0 g/L) and dosage of (c) MCC-g-AA$_{0.5}$ (C$_i$ 10 mg/L, pH 6) & (d) CS-g-AA$_4$ (C$_i$ 10 mg/L, pH 6).

Analyzing the adsorption kinetics helps in understanding the adsorption mechanism and rate-determining step. The PFO assumes that physisorption is the rate-determining step whereas the PSO assumes that chemisorption is the rate-determining step (Mousavi et al. 2023). Figure 11 shows the fitting curves of the PFO and PSO models to the experimental kinetic data and Table 1 gives the obtained parameters of these models.

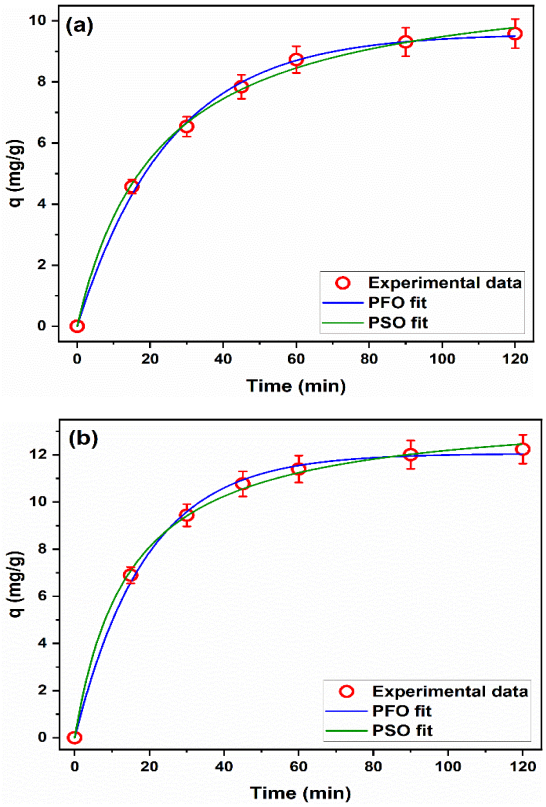

Figure 11. Kinetics of adsorption of RhB onto (a) MCC-g-AA$_{0.5}$ (C$_i$ 10 mg/L, dosage 1.0 g/L, pH$_i$ 6) and (b) CS-g-AA$_4$ (C$_i$ 10 mg/L, dosage 0.5 g/L, pH$_i$ 6).

A visual inspection of Figure 11 shows that the experimental data can be well-fitted to both PFO and PSO models. This observation is corroborated by the numerical data in Table 1, where the R^2 of both PFO and PSO are greater than 0.999. This outcome implies that the adsorption process includes several mechanisms. A similar outcome has been reported before [21,33] Comparing the values χ^2 for the PFO and PSO models can expose which model can give a better fit to the experimental data, the lower χ^2 the better fit. The χ^2 values in Table 1 expose that the PSO and PFO models describe the kinetics of adsorption of RhB onto MCC-g-AA$_{0.5}$ and CS-g-AA$_4$ marginally better than the PFO and PSO models, respectively. Thus, it can be said that physisorption and chemisorption are both involved in the adsorption of RhB, with chemisorption predominating in the case of MCC-g-AA$_{0.5}$ and, physisorption in the case of CS-g-AA$_4$.

Table 1. Values of the fitting parameters of the PFO and PSO kinetic models.

	MCC-g-$AA_{0.5}$		CS-g-AA_4	
	PFO	**PSO**	**PFO**	**PSO**
R^2	0.99998	0.99999	0.99999	0.99999
χ^2	0.03973	0.03114	0.02298	0.02867
k	0.05 ± 0.002	0.005 ± 0.0004	0.040 ± 0.002	0.004 ± 0.0004
q_e	12.06 ± 0.130	13.97 ± 0.21	9.580 ± 0.119	11.60 ± 0.25

Studying the adsorption isotherm provides insights about the relation between the initial concentration of RhB and the amount adsorbed at equilibrium, the mechanism of the adsorption process, the nature of the adsorbent and the theoretical maximum adsorption capacity of the adsorbent. Herein, the experimental adsorption isotherm was analyzed by Freundlich and Langmuir models. Figure 12 depicts the experimental and Freundlich and Langmuir fitted isotherm models. As seen in Figure 12, the amount adsorbed of RhB continuously increase with increasing the initial concentration. When the initial concentration of RhB increases, both the concentration gradient near the adsorbent and the collisions between RhB molecules increase. Consequently, the rate of diffusion of RhB molecules to the surface of the adsorbent increases which eventually results in the observed increase in the amount of adsorbed RhB.

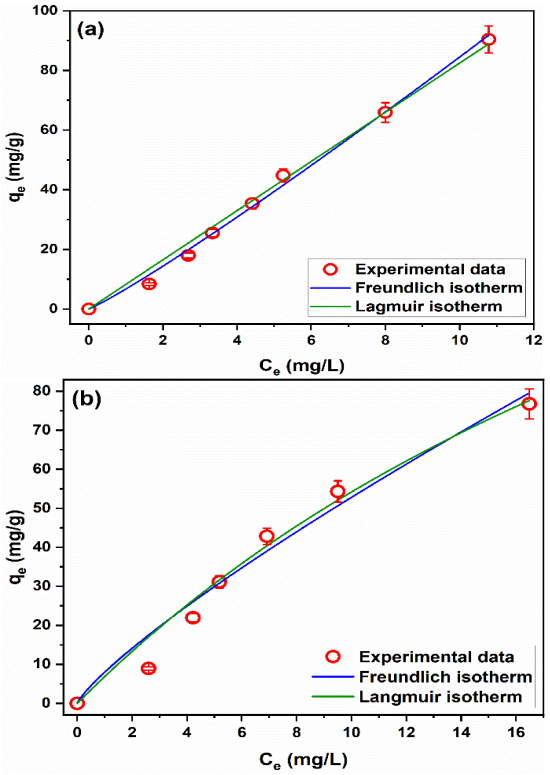

Figure 12. Adsorption isotherms of RhB onto (a) MCC-g-$PAA_{0.5}$ (dosage 1.0 g/L, pH_i 6, contact time 3 hr) and (b) CS-g-PAA_4 (dosage 0.75 g/L, pH_i 6, contact time 2 hr).

Figure 12 also illustrates that both Freundlich and Langmuir isotherm models fit well the experimental adsorption isotherm of RhB onto MCC-g-$AA_{0.5}$ and CS-g-AA_4. To validate this observation the isotherm parameters were calculated and are listed in Table 2. The values of R^2 for both Freundlich and Langmuir isotherm models are greater than 0.999 which verifies that they fit the experimental data well. This observation agrees with precedent reports where fitting of several different isotherm models to experimental data have been reported before [21,25,35,37-39]. Moreover, this observation supports the outcome of the kinetic study that several mechanisms are involved in the adsorption process.

Table 2. Values of the fitting parameters of Freundlich and Langmuir isotherm models.

MCC-g-$PAA_{0.5}$			
Freundlich		**Langmuir**	
R^2	0.99994	R^2	0.99988
χ^2	0.06625	χ^2	0.12744
K_F	6.71 ± 0.62	K_L	2.85 x 10^{-5} ± 0.01
n_F	0.91 ± 0.04	q_L	289589.58 ± 8.34 x 10^7
CS-g-PAA_4			
Freundlich		**Langmuir**	
R^2	0.99936	R^2	0.99960
χ^2	0.89354	χ^2	0.55974
K_F	7.98 ± 1.79	K_L	0.03 ± 0.01
n_F	1.22 ± 0.13	q_L	233.03 ± 65.04

The values of χ^2 in Table 2 illustrate that Freundlich model describes the adsorption isotherm of RhB onto MCC-g-$AA_{0.5}$ slightly better than Langmuir model. Also, though the values of R^2 and χ^2 suggest that the Langmuir can describe the adsorption isotherm of RhB onto MCC-g-$AA_{0.5}$, the values of K_L and q_L appear illogical which rules out the applicability of Langmuir model to the experimental data. Freundlich model is designed to describe the non-ideal multilayer adsorption onto heterogeneous surfaces where the adsorbates interact with each other [28]. Thus, it can be deduced that the surface of MCC-g-$AA_{0.5}$ contains adsorption sites with various energies and that the adsorbed RhB forms multilayer onto MCC-g-$AA_{0.5}$. On the other side, according to the values of χ^2 the adsorption isotherm of RhB onto CS-g-AA_4 is better described by Langmuir model. Langmuir model is designed to describe monolayer of non-interacting adsorbates

onto an adsorbent that contains adsorption sites with equal adsorption energies [29]. Accordingly, the adsorption sites on the surface of CS-g-PAA_4 have equal energies, RhB forms monolayer on the surface of CS-g-PAA_4 and adsorbed RhB do not interact with each other.

The theoretical monolayer saturation capacity is a characteristic parameter of Langmuir model and is widely used to compare the efficacy of adsorbents reported in the literature toward a specific adsorptive. Table 3 lists some of the reported Langmuir theoretical monolayer saturation capacity of several adsorbents toward RhB.

Table 3. Langmuir theoretical monolayer adsorption capacity of different adsorbents toward RhB.

Adsorbent	q_L (mg/g)
Activated carbon from cement waste [40]	531.84
Modified bentonite [41]	284.4
Chitosan modified with 2,3-dihydroxy-benzaldehyde [42]	233.40
CS-g-PAA_4 (This work)	***233.03***
SnS_2 [43]	200
Modified NH-bentonite [44]	192.3
Sodium tauroglycocholate functionalized mesoporous silica nanoparticles [22]	173.96
Carbon xerogel modified with ethylenediamine [45]	132
Java bentonite [44]	116.3
Mesoporous NiO nanoparticles [46]	111
Activated carbon from Samanea saman waste pods [47]	101.01
Polyaniline-coated porous and fibrous nanocomposite [48]	34.93
Moroccan natural clay bentonite [49]	29.33
Oligocyclopentadiene resin [50]	17.80
Kaolin-organic bentonite [51]	12.68
Fe–N co-modified biochar [52]	12.41
Kaolin [51]	7.760
Pomegranate peels ground powder [53]	7.370
Zeolite [25]	6.964
Acid-activated halloysite [50]	6.290
Stalk corn activated carbon [20]	5.3
Halloysite [25]	4.252
Chalcedonite [25]	2.701
Raw walnut shells [54]	2.292
Silica particles derived from natural kaolinite [55]	1.70
Sugar cane bagasse [56]	1.250
Devonian sand [25]	0.349

Table 3 reveals that the q_L of CS-g-AA_4 is higher than a lot of other reported adsorbents in the literature. However, few other adsorbents such as activated carbon from cement waste [41] and modified bentonite [43] have higher adsorption capacity than CS-g-AA_4. Overall, it can be inferred from Table 3 that CS-g-AA_4 has good adsorption capacity and can be considered a promising candidate for removing organic dyes from wastewater.

Conclusions

As comparison study between CS-g-AA and MCC-g-AA on adsorption of RhB as representative for cationic dyes show that there is no significant difference in adsorption rate which prove that the using of waste biomass or waste stalk is costly effective, easier, faster, excessive compassion with same result in comparative.

Globally, a great deal of research is being done to create new materials that combine raw materials from renewable, natural sources with biodegradability. Several cellulose sources, such as maize stalk waste, were generated by copolymerization via free radical grafting and employed as superabsorbent co-polymers utilizing acrylic acid. The crosslinking agent employed in the syntheses was hydrophilic N,N'-methylenebisacrylamide, and the initiators used were ammonium persulfate. It was discovered by FTIR and SEM analyses that AA monomers had been grafted onto the macromolecular chains of CS. For the grafting of microcrystalline cellulose MCC and product characterisation, a comparative experiment was conducted.

Detailed adsorption study was performed using RhB as representative for cationic dyes and included the evaluation of the adsorption performance of all the prepared materials, assessing the effect of initial pH of RhB solution, and adsorbent dosage. Furthermore, the adsorption kinetics and isotherm studies were performed. The kinetic data was analyzed using the pseudo-first-order and pseudo-second-order models while the isotherm data was analyzed using Freundlich and Langmuir models. The results showed that pH affects the removal of RhB by MCC-g-$AA_{0.5}$ and has insignificant effect when CS-g-AA_4 was used. The adsorption kinetic followed both the pseudo-first-order and pseudo-second-order models with the predominance of the pseudo-second-order in case of MCC-g-$AA_{0.5}$ and pseudo-first-order in case of CS-g-PAA_4. Similarly, both Freundlich and Langmuir models fitted the experimental adsorption isotherm well with the predominance of Freundlich in case of MCC-g-$AA_{0.5}$ and Langmuir in case of CS-g-AA_4.

A comprehensive comparison of the Langmuir theoretical monolayer saturation capacity of CS-g-AA_4 with literature revealed its high promise for the removal of RhB from contaminated aqueous

Authors sincerely appreciate The 6th Chemical Industrial Research Institute Conference (CIRIC-6)

The authors gratefully acknowledge National Research Centre, for financial support for facilities provided through project ID: 13010406

Reference

1- Ates B, Koytepe S, Ulu A, Gurses C, Thakur VK. Chemistry, Structures, and Advanced Applications of Nanocomposites from Biorenewable Resources. Chem Rev 2020;120:9304–62. https://doi.org/10.1021/acs.chemrev.9b00553.

2- Siwal SS, Zhang Q, Devi N, Saini AK, Saini V, Pareek B, et al. Recovery processes of sustainable energy using different biomass and wastes. Renewable and Sustainable Energy Reviews 2021;150:111483. https://doi.org/10.1016/j.rser.2021.111483.

3- K. Rana A, Kumar Thakur V. The bright side of cellulosic hibiscus sabdariffa fibres: towards sustainable materials from the macro- to nano-scale. Materials Advances 2021. https://doi.org/10.1039/D1MA00429H.

4- Voicu SI, Thakur VK. Aminopropyltriethoxysilane as a linker for cellulose-based functional materials: New horizons and future challenges. Current Opinion in Green and Sustainable Chemistry 2021;30:100480. https://doi.org/10.1016/j.cogsc.2021.100480.

5- Ahmed, A. S., El-Masry, A. M., Saleh, A., & Nada, A. (2013). Bagasse hydrogels: water absorption and ions uptake. Pigment & Resin Technology, 42(1), 68-78.

6- Binchan Zhaoa, Huabin Jianga, Zongkun Lina, Shaofan Xua, Jun Xiea, Aiping Zhang Preparation of acrylamide/acrylic acid cellulose hydrogels for the adsorption of heavy metal ions Carbohydrate Polymers 224 (2019) 115022

7- Heverton Michael Biazzi; Jiovani Sergio Bee Tubin; Renato Augusto Conte; Weber da Silva Robazza; Different sieving methods for determining the physical characteristics in ground corn Diovani Paiano Acta Scientiarum. Animal Sciences, vol. 44, e53382, 2022

8- Mo J., Yang Q., Zhang N., Zhang W., Zheng Y., Zhang Z. A review on agro-industrial waste (AIW) derived adsorbents for water and wastewater treatment. J. Environ. Manage., 2018; 227: 395–405. doi:10.1016/j.jenvman.2018.08.069.

9- Yadav S., Yadav A., Bagotia N., Sharma A. K., Kumar S. Adsorptive potential of modified plant-based adsorbents for sequestration of dyes and heavy metals from wastewater-a review. J. Water Process. Eng., 2021; 42: 102148. doi:10.1016/j.jwpe.2021.102148.

10- Khattri S., Singh M. Removal of malachite green from dye wastewater using neem sawdust by adsorption. J. Hazard. Mater., 2009; 167(1–3): 1089–1094. doi:10.1016/j.jhazmat.2009.01.101.

11- Tao H.-C., Zhang H.-R., Li J.-B., Ding W.-Y. Biomass based activated carbon obtained from sludge and sugarcane bagasse for removing lead ion from wastewater. Bioresour. Technol., 2015; 192: 611–617. doi:10.1016/j.biortech.2015.06.006.

12- Ahmaruzzaman M., Gupta V. K. Rice husk and its ash as low-cost adsorbents in water and wastewater treatment. Ind. Eng. Chem. Res., 2011; 50(24): 13589–13613. doi:10.1021/ie201477c.

13- Basta A. H., El-Saied H., El-Hadi O., El-Dewiny C. Evaluation of rice straw-based hydrogels for purification of wastewater. *Polym.-Plast. Technol. Eng.*, 2013; 52(11): 1074–1080. doi:10.1080/03602559.2013.806548.

14- Zhou Q., Yan C., Luo W. Preparation of a novel carboxylate-rich wheat straw through surface graft modification for efficient separation of Ce (III) from wastewater. *Mater. Des.*, 2016; 97: 195–203. doi:10.1016/j.matdes.2016.02.081.

15- Janoš P., Coskun S., Pilařová V., Rejnek J. Removal of basic (Methylene Blue) and acid (Egacid Orange) dyes from waters by sorption on chemically treated wood shavings. *Bioresour. Technol.*, 2009; 100(3):1450–1453. doi:10.1016/j.biortech.2008.06.069.

16- Gong R., Sun Y., Chen J., Liu H., Yang C. Effect of chemical modification on dye adsorption capacity of peanut hull. *Dyes Pigm.*, 2005; 67(3): 175–181. doi:10.1016/j.dyepig.2004.12.003.

17- Synthesis of Corn Starch Derivatives and Their Application in Yarn Sizing Stana Kovac˘evic´ 1 , Ivana Schwarz 1,* , Suzana Đord¯evic´ 2 and Dragan Đord¯evic´ 3 Polymers 2020, 12, 1251

18- Studies on Graft Copolymerization of Acrylic Acid onto Acetylate Cellulose from Maize Cob Aliyu Danmusa Mohammed* and Aisha Kabir Ahmed Mohammed AD, Ahmed AK. JOTCSA. 2022; 9(2): 571-578.

19- Dual-Grafting of Microcrystalline Cellulose by Tea Polyphenols and Cationic ε-Polylysine to Tailor a Structured Antimicrobial Soy-Based Emulsion for 3D Printing Mahdiyar Shahbazi,* Henry Jäger,* and Rammile Ettelaie ACS Appl. Mater. Interfaces 2022, 14, 21392−21405 https://doi.org/10.1021/acsami.1c19430

20- Mousavi SA et al. (2023) Removal of Rhodamine B from aqueous solution by stalk corn activated carbon: adsorption and kinetic study Biomass Conversion and Biorefinery 13:7927-7936 doi:10.1007/s13399-021-01628-1

21- Radwan EK, Hemdan BA, El-Wakeel ST, Omar RA, Rashdan HRM, El-Naggar ME (2024) Synthesis and application of a new multi-functional biopolymer-based aerogel loaded with bistriazole derivative as highly efficient adsorbent and disinfectant Journal of Cleaner Production 434:139932 doi:https://doi.org/10.1016/j.jclepro.2023.139932

22- Alswieleh AM (2023) Kinetic, equilibrium and thermodynamic studies for rhodamine B adsorption on sodium tauroglycocholate functionalized mesoporous silica nanoparticles Journal of Porous Materials 30:937-948 doi:10.1007/s10934-022-01395-y

23- Guo S et al. (2023) Synergistic effect of hydrogen bonding and π-π interaction for enhanced adsorption of rhodamine B from water using corn straw biochar Environmental Pollution 320:121060 doi:https://doi.org/10.1016/j.envpol.2023.121060

24- Mansor ES, El Shall FN, Radwan EK (2023) Simultaneous decolorization of anionic and cationic dyes by 3D metal-free easily separable visible light active photocatalyst Environ Sci Pollut Res Int 30:10775-10788 doi:10.1007/s11356-022-22838-8
25- Kuśmierek K, Fronczyk J, Świątkowski A (2023) Adsorptive Removal of Rhodamine B Dye from Aqueous Solutions Using Mineral Materials as Low-Cost Adsorbents Water, Air, & Soil Pollution 234:531 doi:10.1007/s11270-023-06511-5
26- Langergren S, Svenska BK (1898) Zur theorie der sogenannten adsorption geloester stoffe Veternskapsakad Handlingar 24:1-39
27- Blanchard G, Maunaye M, Martin G (1984) Removal of heavy metals from waters by means of natural zeolites Water Research 18:1501-1507 doi:https://doi.org/10.1016/0043-1354(84)90124-627-Freundlich HMF (1906) Over the adsorption in solution Journal of Physical Chemistry 57: 385-470
28- Freundlich HMF (1906) Over the adsorption in solution Journal of Physical Chemistry 57: 385-470
29- Langmuir I (1918) The adsorption of gases on plane surfaces of glass, mica and platinum Journal of the American Chemical society 40:1361-1403
30- -Grafting Starch with Acrylic Acid and Fenton's Initiator: The Selectivity Challenge Inge-Willem Noordergraaf 1,*, Judy R. Witono 2 and Hero J. Heeres 1 doi: 0.20944/preprints202310.0022.v1
31- Dashairya L, Sharma S, Rathi A, Saha P, Basu S (2021) Solar-light-driven photocatalysis by Sb2S3/carbon based composites towards degradation of noxious organic pollutants Materials Chemistry and Physics 273:125120 doi:https://doi.org/10.1016/j.matchemphys.2021.125120
32- El Bendary MM, Radwan EK, El-Shahat MF (2021) Valorization of secondary resources into silica-based adsorbents: Preparation, characterization and application in dye removal from wastewater Environmental Nanotechnology, Monitoring & Management 15:100455 doi:https://doi.org/10.1016/j.enmm.2021.100455
33- You X et al. (2023) Reinforced Rhodamine B adsorption on the hyper-cross-linked resin co-modified by pyridine and carboxyl groups Microporous and Mesoporous Materials 349:112423 doi:https://doi.org/10.1016/j.micromeso.2022.112423
34- Koryam AA, El-Wakeel ST, Radwan EK, Fattah AMA, Darwish ES (2023) Preparation and characterization of chemically cross-linked zwitterionic copolymer hydrogel for direct dye and toxic trace metal removal from aqueous medium Environmental Science and Pollution Research doi:10.1007/s11356-023-26966-7
35- Abrishamkar S, Mohammadi A, De La Vega J, Wang D-Y, Kalali EN (2023) Layer-by-layer assembly of calixarene modified GO and LDH nanostructures on flame retardancy, smoke suppression, and dye adsorption behavior of flexible polyurethane foams Polymer Degradation and Stability 207:110242 doi:https://doi.org/10.1016/j.polymdegradstab.2022.110242
36- Akiode OK, Adetoro A, Anene AI, Afolabi SO, Alli YA (2023) Methodical study of chromium (VI) ion adsorption from aqueous solution using low-cost agro-waste material: isotherm, kinetic, and thermodynamic studies Environmental Science and Pollution Research 30:48036-48047 doi:10.1007/s11356-023-25706-1
37- El Malah T, Nour HF, Radwan EK, Abdel Mageid RE, Khattab TA, Olson MA (2021) A bipyridinium-based polyhydrazone adsorbent that exhibits ultrahigh adsorption capacity for the anionic azo dye, direct blue 71 Chemical Engineering Journal 409:128195 doi:https://doi.org/10.1016/j.cej.2020.128195
38- Mirzaei K, Jafarpour E, Shojaei A, Khasraghi SS, Jafarpour P (2023) An investigation on the influence of highly acidic media on the microstructural stability and dye adsorption performance of UiO-66 Applied Surface Science 618:156531 doi:https://doi.org/10.1016/j.apsusc.2023.156531
39- Rubangakene NO, Elwardany A, Fujii M, Sekiguchi H, Elkady M, Shokry H (2023) Biosorption of Congo Red dye from aqueous solutions using pristine biochar and ZnO biochar from green pea peels Chemical Engineering Research and Design 189:636-651 doi:https://doi.org/10.1016/j.cherd.2022.12.003
40- da Silva WL, Muraro PCL, Pavoski G, Espinosa DCR, dos Santos JHZ (2022) Preparation and characterization of biochar from cement waste for removal of rhodamine B dye Journal of Material Cycles and Waste Management 24:1333-1342
41- de Morais Pinos JY, de Melo LB, de Souza SD, Marçal L, de Faria EH (2022) Bentonite functionalized with amine groups by the sol-gel route as efficient adsorbent of rhodamine-B and nickel (II) Applied Clay Science 223:106494 doi:https://doi.org/10.1016/j.clay.2022.106494
42- Alakhras F, Ouachtak H, Alhajri E, Rehman R, Al-Mazaideh G, Anastopoulos I, Lima EC (2022) Adsorptive Removal of Cationic Rhodamine B Dye from Aqueous Solutions Using Chitosan-Derived Schiff Base Separation Science and Technology 57:542-554 doi:10.1080/01496395.2021.1931326
43- Wang S, Yang B, Liu Y (2017) Synthesis of a hierarchical SnS2 nanostructure for efficient adsorption of Rhodamine B dye Journal of Colloid and Interface Science 507:225-233 doi:https://doi.org/10.1016/j.jcis.2017.07.053
44- Hakim YM, Mohadi R, Mardiyanto M, Royani I (2023) Ammonium-Assisted Intercalation of Java Bentonite as Effective of Cationic Dye Removal Journal of Ecological Engineering 24:184-195 doi:10.12911/22998993/156665
45- Ptaszkowska-Koniarz M, Goscianska J, Pietrzak R (2018) Removal of rhodamine B from water by modified carbon xerogels Colloids and Surfaces A: Physicochemical and Engineering Aspects 543:109-117 doi:https://doi.org/10.1016/j.colsurfa.2018.01.057
46- Motahari F, Mozdianfard MR, Salavati-Niasari M (2015) Synthesis and adsorption studies of NiO nanoparticles in the presence of H2acacen ligand, for removing Rhodamine B in wastewater treatment Process Safety and Environmental Protection 93:282-292 doi:https://doi.org/10.1016/j.psep.2014.06.006
47- Kumbhar P, Patil S, Narale D, Sartape A, Jambhale C, Kim J-H, Kolekar S (2022) Biobased carbon for

effective removal of rhodamine B and Cr(VI) from aqueous solution: kinetic, isotherm and thermodynamic study Biomass Conversion and Biorefinery doi:10.1007/s13399-022-02625-8
48- Meena PL, Saini JK, Surela AK, Poswal K, Chhachhia LK (2022) Fabrication of polyaniline-coated porous and fibrous nanocomposite with granular morphology using tea waste carbon for effective removal of rhodamine B dye from water samples Biomass Conversion and Biorefinery:1-20
49- Lamrani O, Tanji K, Redouane H, Fahoul Y, Belkasmi M, Boushaba A (2023) Efficient adsorption of RhB using Moroccan natural clay: equilibrium, kinetic, thermodynamic, and theoretical study Euro-Mediterranean Journal for Environmental Integration 8:303-318 doi:10.1007/s41207-023-00380-4
50- Wierzbicka E, Kuśmierek K, Świątkowski A, Legocka I (2022) Efficient Rhodamine B Dye Removal from Water by Acid- and Organo-Modified Halloysites Minerals 12:350
51- He H, Chai K, Wu T, Qiu Z, Wang S, Hong J (2022) Adsorption of Rhodamine B from Simulated Waste Water onto Kaolin-Bentonite Composites Materials 15:4058
52- Li X, Shi J, Luo X (2022) Enhanced adsorption of rhodamine B from water by Fe-N co-modified biochar: Preparation, performance, mechanism and reusability Bioresource Technology 343:126103 doi:https://doi.org/10.1016/j.biortech.2021.126103
53- Saigl ZM, Ahmed AM (2021) Separation of Rhodamine B dye from aqueous media using natural pomegranate peels Indonesian Journal of Chemistry 21:212-224
54- Shah J, Rasul Jan M, Haq A, Khan Y (2013) Removal of Rhodamine B from aqueous solutions and wastewater by walnut shells: kinetics, equilibrium and thermodynamics studies Frontiers of Chemical Science and Engineering 7:428-436 doi:10.1007/s11705-013-1358-x
55- Celoria G, Miglio V, Paul G, Bisio C, Golemme G, Boccaleri E (2022) Silica Particles Derived from Natural Kaolinite for the Removal of Rhodamine B from Polluted Water Processes 10:964
56- Abou Gamra Z, Medien H (2013) Kinetic, thermodynamic and equilibrium studies of Rhodamine B adsorption by low cost biosorbent sugar cane bagasse Eur Chem Bull 2:417-422